Solvent immersion nanoimprint lithography of fluorescent conjugated polymers

G. L. Whitworth, S. Zhang, J. R. Y. Stevenson, B. Ebenhoch, I. D. W. Samuel, and G. A. Turnbull

Solvent immersion nanoimprint lithography of fluorescent conjugated polymers

G. L. Whitworth, S. Zhang,[a] J. R. Y. Stevenson, B. Ebenhoch, I. D. W. Samuel, and G. A. Turnbull
Organic Semiconductor Centre, SUPA, School of Physics and Astronomy, University of St Andrews, St Andrews KY16 9SS, United Kingdom

Solvent immersion imprint lithography (SIIL) was used to directly nanostructure conjugated polymer films. The technique was used to create light-emitting diffractive optical elements and organic semiconductor lasers. Gratings with lateral features as small as 70 nm and depths of ~25 nm were achieved in poly(9,9-dioctylfluorenyl-2,7-diyl). The angular emission from the patterned films was studied, comparing measurement to theoretical predictions. Organic distributed feedback lasers fabricated with SIIL exhibited thresholds for lasing of ~40 kW/cm^2, similar to those made with established nanoimprint processes. The results show that SIIL is a quick, convenient and practical technique for nanopatterning of polymer photonic devices. © 2015 AIP Publishing LLC. [http://dx.doi.org/10.1063/1.4933316]

The simple processing and high photoluminescence (PL) efficiency of semiconducting light-emitting polymers make them attractive materials for inexpensive photonic and optoelectronic devices. They have been used in a wide range of applications including organic light-emitting diodes (OLEDs),[1,2] light-emitting field-effect transistors (LEFETs),[3] optically pumped organic semiconductor lasers (OSLs),[4–7] and colour converters in visible light communications.[8] Wavelength scale microstructures have been used to control PL emission and functionality in planar devices; for example, distributed feedback (DFB) gratings are used to create optical resonators in OSLs and nanostructures can be used to create directional emission from OLEDs.[9]

For such applications, there are several benefits to have the active layer itself patterned as opposed to coating the light emitting film on a nanostructured substrate. For example, nanostructures made out of the emitting material can take advantage of the greater refractive index contrast between the polymer (n ~ 1.6–1.9) and air at the patterned interface, leading to greater diffraction efficiencies. This architecture can also be implemented on any substrate allowing easy integration into optoelectronic devices. Many standard lithography techniques for producing DFB gratings such as ultraviolet nanoimprint lithography (UV-NIL)[10,11] and holographic polymerisation[12] need to be implemented in specialised resist layers, therefore do not generally achieve the aforementioned desirable device structure.[13] Hot embossing/thermal nanoimprinting has been successfully shown to meet these requirements;[14,15] however these processes involve heating a polymer above its glass transition temperature (~200 °C), which can potentially damage the emission efficiency of the polymer or cause it to crystallise upon subsequent cooling, and can also be incompatible with processing on some flexible substrates or in multilayer device architectures.

Recently, a new imprinting technique was reported by Vasdekis *et al.*, solvent immersion imprint lithography (SIIL),[16] which was used to create microfluidic channels. This is a solvent based method in which polymer films are converted into malleable surface "gels," which can then be deformed into a desired structure via soft lithographic imprinting. SIIL was shown to be an improvement on related methods to replicate micron scale topographies such as solvent assisted micro-moulding (SAMiM),[17] by producing deeper, higher quality imprints. The process is also fully scalable and open to the possibility of industrial expansion via roll-to-roll printing. In this paper, we adapt this technique to form structures on the nanometer scale (with features as small as 70 nm), directly into a fluorescent conjugated polymer. The nanopatterning technique is used to form directional polymer light emitters and OSLs.

The commercially available conjugated polymer Poly(9,9-dioctylfluorenyl-2,7-diyl) (PFO) (Lumtec, Inc.) (M$_W$ = 51506 g/mol) was used as the basis of our devices. PFO films were fabricated by spin-coating a 20 mg/ml toluene solution onto a glass substrate, which had been pretreated with an adhesion promoter (mr-APS1 from Microresist Technology (~4 nm thick)). PL from the films (~250 nm thick) was measured using a 355 nm diode-pumped solid-state (DPSS) passively Q-switched laser excitation source (FTSS355-Q2-OEM, CryLas GmbH) and a fibre-coupled CCD spectrometer. The PL spectrum is shown in Fig. 1(a) and is composed of several vibronic emission peaks at 434 nm, 461 nm, 495 nm, and 530 nm. Amplified spontaneous emission (ASE) spectra were measured by focusing the pump laser to a 4 mm × 0.5 mm stripe onto the surface of an unpatterned planar film using a cylindrical lens. Light emission was collected from the edge of the film at high pump power density, using the CCD spectrometer. The resulting ASE spectrum (shown in Fig. 1(a)) has a single narrow peak with a FWHM of 5 nm, centred at 463 nm close to the 0–1 emission peak of the PL spectrum.[18]

The films were nanopatterned by SIIL using a perfluoropolyether soft stamp. The soft stamps (MD700 (Solvay))

---

[a]Present address: School of Information Science and Technology, Fudan University, Shanghai 200433, China.
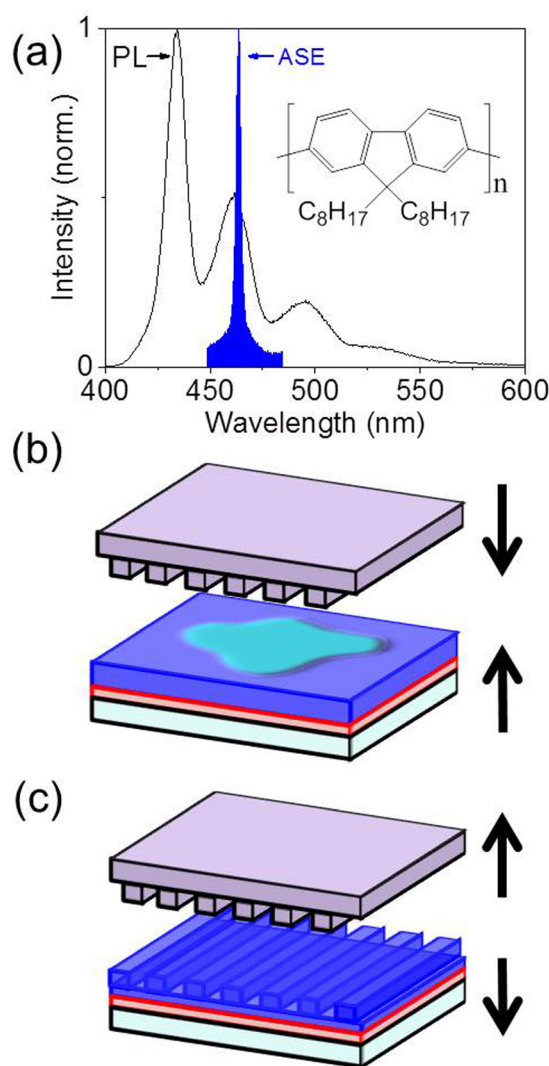
FIG. 1. (a) Normalised photoluminescence spectrum of PFO and the amplified spontaneous emission spectrum taken at high pump power density. The inset shows the chemical structure of PFO. (b) The first part of the SIIL process in which a soft stamp is pressed into an acetone soaked PFO film. (c) The second part of the SIIL process in which the stamp is separated from the film to leave behind a nanostructured PFO film.

were cast on silicon master gratings (patterned by e-beam lithography and reactive ion etching), and hardened by ultraviolet curing. A drop of acetone ($\sim$100 μl) was placed on the surface of the PFO film. The acetone infiltrates into the film forming a surface "gel," but does not dissolve the polymer. The MD700 stamp was immediately pressed into the surface using an EVG 620 photomask aligner with custom NIL tooling to achieve a constant uniform pressure of 950 mbar.[11] A range of imprint times from 1 s to 120 s were tested. No difference was seen in the structures for this range, but the longest time (120 s) was chosen to ensure maximum removal of excess acetone. While in contact, the acetone diffuses into the soft stamp, thereby removing it from the film. When the soft stamp was removed, the PFO surface was left structured with a replica of the silicon master grating. The mr-APS1 layer was required so that the PFO did not adhere to the stamp surface but instead remained on the glass substrate. PL quantum yield (PLQY) was measured before and after imprinting using a Hamamatsu integrating sphere.[19] The PLQY increased notably from 41% to 54% when films were

treated with acetone due to a modification of molecular morphology.[20]

Several different grating designs were imprinted into the PFO films. Fig. 2 shows SEM and AFM images of nanopatterns formed into PFO using SIIL, including (a) 1D and (b) 2D gratings. The 1D grating has regions with periods of 140 nm and 280 nm, with a minimum feature size of 70 nm. 2D nano-pillar arrays were also fabricated with a 280 nm lattice constant in both *x* and *y* dimensions. Fig. 2(c) shows an AFM image of the 2D grating, with a uniform imprinting depth of 23 nm. When imprinting films using other polymers of lower molecular weight, gratings as deep as 80 nm were achieved, matching the feature depth on the MD700 stamp.

The wavelength-scale nanostructures can strongly affect the light emission from the polymer film. The angular distribution of PL from the imprinted films was investigated using a Radiant Vision Systems imaging sphere, which measures the light emission profile across a hemisphere and plots the data as a 2D polar projection. Limited spectral information can be obtained by using the built-in red, green, and blue colour filters, which have transmissions matching the CIE standard
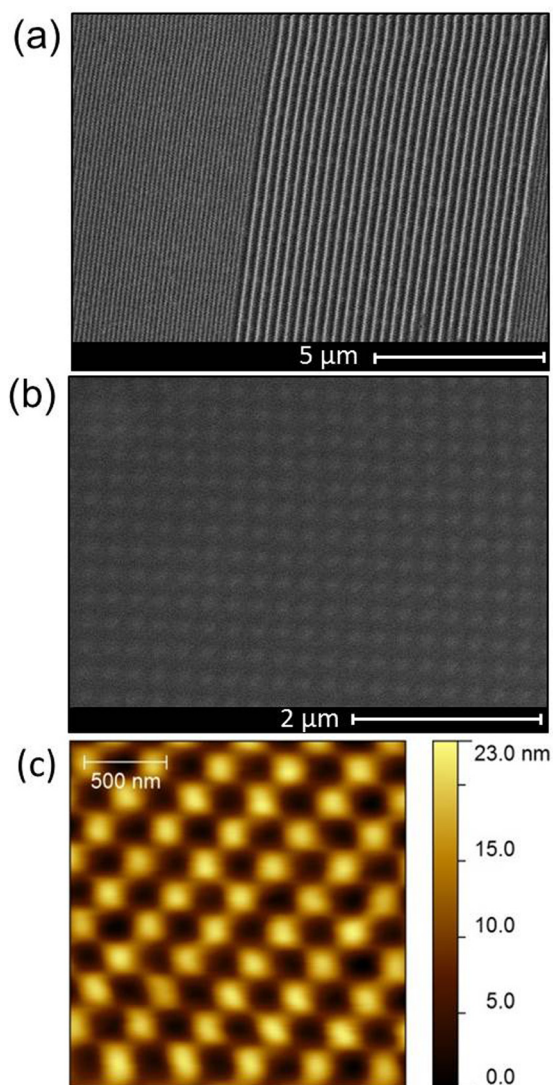

FIG. 2. (a) and (b) SEM images of PFO gratings. (a) A 1D grating with a mixed period (140 nm and 280 nm). (b) A 2D PFO grating with a lattice constant of 280 nm. (c) AFM image of the grating in (b).

observer functions. Fig. 3(a) shows the measurement angle geometry relative to the grating grooves. Figs. 3(b)–3(d) show false colour polar plots of the emission from 2D structured PFO films transmitted through (b) blue, (c) green, and (d) red filters, detected by the imaging sphere. The radial axis represents the emission angle θ between 0° and 85°, and the false colour shows the luminous intensity emitted at that angle. The angular axis φ is the azimuthal angle in the sample plane, as shown in Fig. 3(a). A grating period of 280 nm was chosen such that the blue PL was strongly forward scattered out of the film, with longer wavelength emission diffracted at higher angles. Fig. 3(b) shows that blue PL was emitted from the film in a cross-like profile with a strong peak normal to the surface of the emitting film. Green PL (Fig. 3(c)) is diffracted out in a square-like pattern with vertices emitted at a 20° angle and red PL (Fig. 3(d)) further still with intensity peaks at 30°.

To understand the wavelength dependent emission pattern, we modelled the diffraction profile of guided waves in the polymer films. A waveguide mode propagating through the film with a modal wavevector k_{mode} at an angle φ to the grating axis is scattered out at a polar angle θ according to the relation

$$k_{mode}^2 = (mk_x - k_0\sin\theta\cos\varphi)^2 + (nk_y - k_0\sin\theta\sin\varphi)^2,$$
(1)

where k_x and k_y are the orthogonal grating vectors, k_0 is the wavenumber, and m and n are the orders of scattering. Solving this for the first order scatterings ($m = 1$, $n = 0$ and $m = 0$, $n = 1$), we can plot the angular emission, $\theta(\varphi)$, for a given wavelength and grating vector.

The peak wavelengths in the transmitted spectra through each of the three bandpass filters were 465, 505, and 540 nm. To obtain the relevant values of $k_{mode}(\lambda)$ for the TE_0 mode, the in-plane refractive indices of the polymer and substrate were first obtained for each wavelength using spectroscopic ellipsometry. A uniaxial refractive index dispersion was required to describe the ellipsometry measurements of PFO, as spin-coated polymers gain a birefringence due to a shear alignment.[21] The in-plane indices of the polymer were 1.864 (at $\lambda = 465$ nm), 1.798 ($\lambda = 505$ nm), and 1.768 ($\lambda = 540$ nm); the refractive indices of the substrate were 1.515, 1.511, and 1.508 at 465, 505, and 540 nm, respectively. Values of $k_{mode}(\lambda)$ were obtained by solving the modal equation for the TE_0 mode, and $\theta(\varphi)$ was then calculated using (1) and compared to the measured angular response. Figs. 3(e)–3(g) show the predicted emission pattern profiles $\theta(\varphi)$, at the three wavelengths of 465, 505, and 540 nm, plotted in polar coordinates to match the representation of the experimental data in Figs. 3(b)–3(d). The blue and green measurements compare well with the calculations, where the predicted emission peaks at 0° and 20° match experiment. $\theta(\varphi)$ for 540 nm predicts scattering to higher angles than those measured. This discrepancy is due to the 5 mm entry aperture of the imaging sphere which only accepted emission angles lower than $\theta = 45$°.

The emission spectrum shows strong spectral dispersion with emission angle. To achieve higher spectrally resolved, angular dependent information, a fibre-coupled spectrometer was used, in which the end of the collection fibre was rotated through θ in the central azimuthal plane. Fig. 4 shows the measured angle-resolved PL emission spectrum for a PFO sample imprinted with a 1D grating of period 280 nm. PL was collected through a linear polariser, orientated either parallel or perpendicular to the grating grooves.

When collecting light polarised perpendicular to the grating, we found that the photoluminescence emission profile of PFO was constant with angle over the range shown in Fig. 4(a). The parallel polarised light however shows a strong dispersion, with a strong forward scattering at $\theta = 0$°. The spectral location of this crossing can be controlled via the grating period and modal wavevector, as shown in Eq. (1). At this intersection of the dispersion curve, the Bragg condition $m\lambda = 2n_{eff}\Lambda$ is satisfied, which gives in-plane distributed feedback of counter propagating waveguide modes, where Λ is the grating period, n_{eff} is the effective refractive index of the mode, and m is the order of diffraction ($m = 2$ for surface emitting DFBs).

Polymer DFB lasers were fabricated by using SIIL and UV-NIL, and the resulting laser performance was compared. UV-NIL gratings were fabricated in a film of UVCur06 (Microresist Technology) using the method detailed by
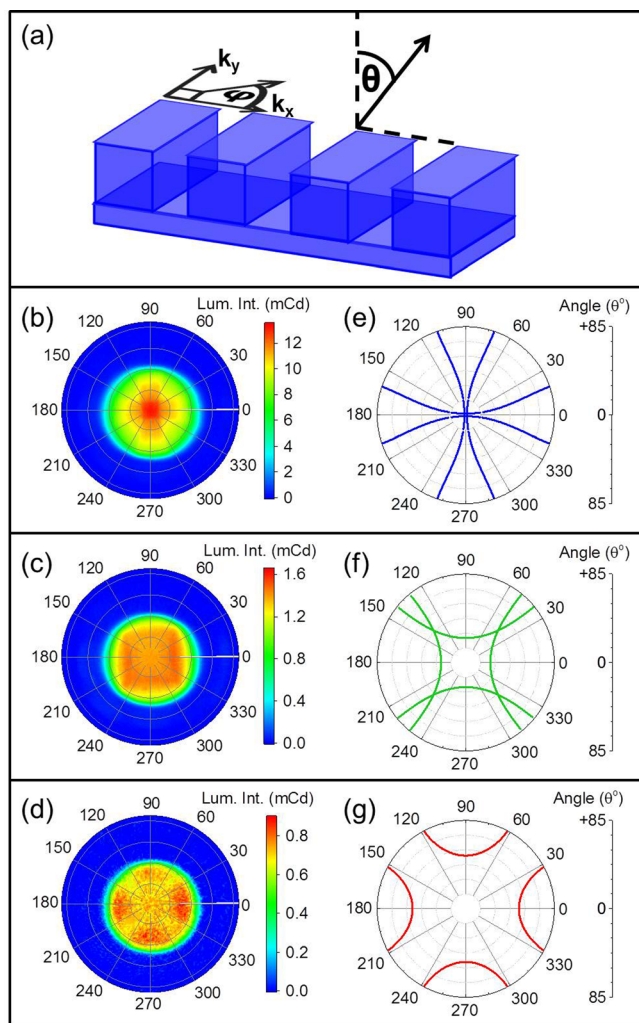

FIG. 3. (a) A schematic defining the angles θ and φ with respect to the polymer nanostructures. (b)–(d) intensity maps of the light emission from PFO films with 2D gratings (280 nm) taken through (b) blue, (c) green, and (d) red colour filters. (e)–(g) Polar plots of the predicted angular emission pattern $\theta(\varphi)$ at wavelengths of (e) 465 nm, (f) 505 nm, and (g) 540 nm.
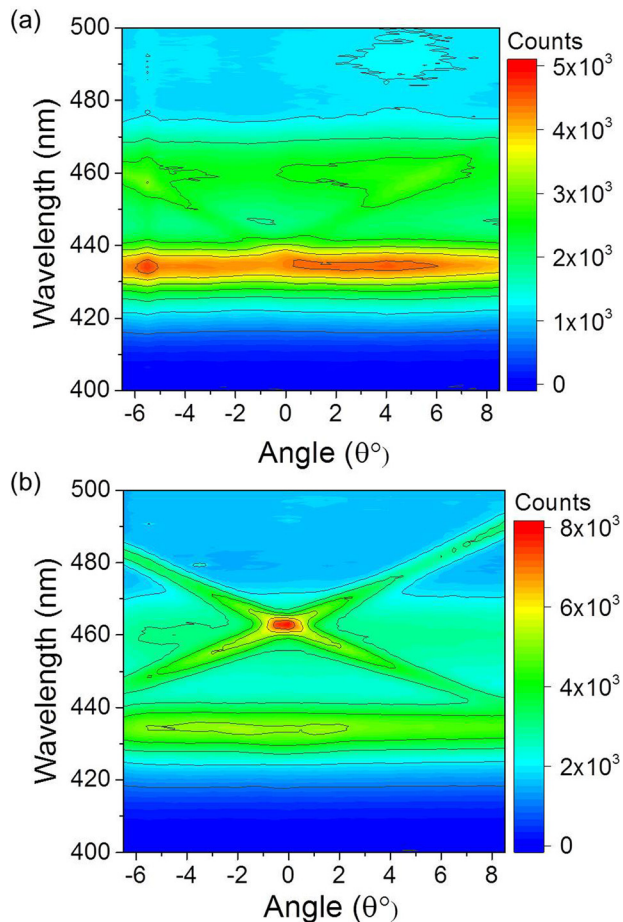
FIG. 4. Angular dependent photoluminescent spectra of a 1D PFO grating (with period 280 nm). Light was collected through a linear polariser where its axis was orientated (a) perpendicular and (b) parallel to the grating grooves.
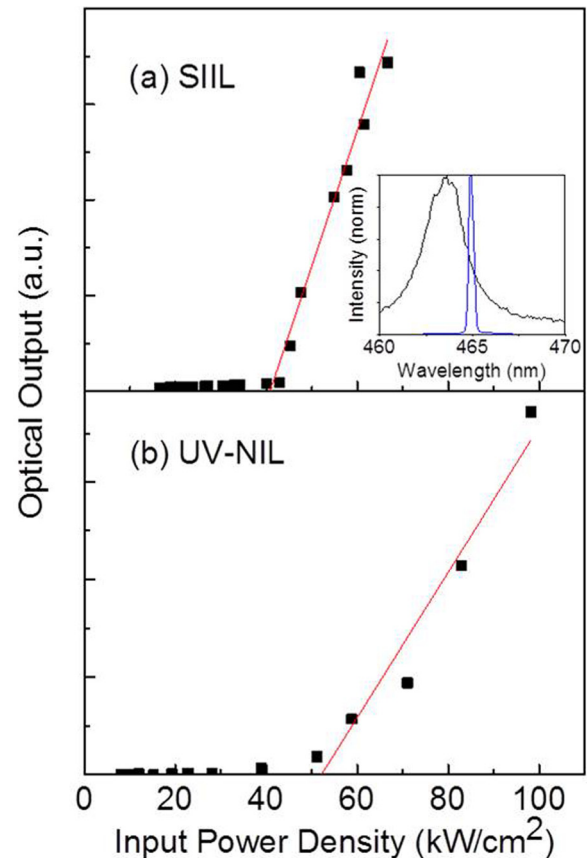

FIG. 5. PFO lasing thresholds of 1D PFO (a) SIIL and (b) UV-NIL gratings. Linear fits are shown for the high energy data points to identify threshold. Inset shows the measured lasing spectra (blue) and the ASE spectra from Fig. 1(a) (black).

Tsiminis *et al.*[11] The PFO films (250 nm) were then spin-cast on top of the UV-NIL grating. The grating depths achieved were $\sim$25 nm and $\sim$80 nm, respectively, for SIIL and UV-NIL methods. A 355 nm DPSS laser at a repetition rate of 100 Hz and pulse duration of 1 ns was focussed to a spot of 1.2 mm diameter onto 1D SIIL and UV-NIL samples. SIIL DFB lasing was achieved at 465 nm (Fig. 5), with a threshold density of $\sim$40 kW/cm^2 (50 nJ/pulse). Despite the smaller grating depths, the SIIL samples showed thresholds similar to lasers made by UV-NIL ($\sim$50 kW/cm^2). A simple finite element analysis model shows that the 9 times smaller over-lap of the shallower SIIL grating with the TE$_0$ mode is compensated by a 2.8 times higher modal gain (due to the simpler waveguide structure) and a 2.3 times higher contrast in dielectric constant at the grating interface.[22] Assuming the laser threshold depends simply on the product of the above three parameters, the SIIL DFB laser should have a threshold of 1.4 times that of the laser made by UV-NIL. This compares well to the ratio of the two measured thresholds of 0.8.

In conclusion, we have presented a simple process for room-temperature nanoimprinting directly into conjugated polymers. The experiments show that a high quality grating can be made with lateral feature sizes as small as 70 nm. Imprinted conjugated polymers showed a strong wavelength dependent, directional emission, with angular profiles consistent with diffraction of waveguided modes from a film. We have also shown that such imprinted devices can easily be made into conjugated polymer solid-state lasers with similar performance to established UV-NIL fabrication. The process has the advantage that diffractive conjugated polymer devices such as lasers can be simply and reliably made on top of a range of substrates, for room temperature integration of photonic nanostructures into optoelectronic devices.

[1]R. H. Friend, R. W. Gymer, A. B. Holmes, J. H. Burroughes, R. N. Marks, C. Taliani, D. D. C. Bradley, D. A. Dos Santos, J. L. Bredas, M. Logdlund, and W. R. Salaneck, Nature **397**, 121 (1999).
[2]C. W. Tang and S. A. Vanslyke, Appl. Phys. Lett. **51**, 913 (1987).
[3]A. Hepp, H. Heil, W. Weise, M. Ahles, R. Schmechel, and H. von Seggern, Phys. Rev. Lett. **91**, 157406 (2003).
[4]I. D. W. Samuel and G. A. Turnbull, Chem. Rev. **107**, 1272 (2007).
[5]S. Chénais and S. Forget, Polym. Int. **61**, 390 (2012).
[6]M. D. McGehee and A. J. Heeger, Adv. Mater. **12**, 1655 (2000).
[7]C. Kallinger, M. Hilmer, A. Haugeneder, M. Perner, W. Spirkl, U. Lemmer, J. Feldmann, U. Scherf, K. Muellen, A. Gombert, and V. Wittwer, Adv. Mater. **10**, 920 (1998).
[8]H. Chun, P. Manousiadis, S. Rajbhandari, D. A. Vithanage, G. Faulkner, D. Tsonev, J. J. D. McKendry, S. Videv, E. Xie, E. Gu, M. D. Dawson, H. Haas, G. A. Turnbull, I. D. W. Samuel, and D. C. O'Brien, IEEE Photonics Technol. Lett. **26**, 2035 (2014).

[9]S. Zhang, G. A. Turnbull, and I. D. W. Samuel, Adv. Opt. Mater. **2**, 343 (2014).

[10]S. Y. Chou, P. R. Krauss, and P. J. Renstrom, Science **272**, 85 (1996).

[11]G. Tsiminis, Y. Wang, A. L. Kanibolotsky, A. R. Inigo, P. J. Skabara, I. D. W. Samuel, and G. A. Turnbull, Adv. Mater. **25**, 2826 (2013).

[12]W. Huang, Z. Diao, Y. Liu, Z. Peng, C. Yang, J. Ma, and L. Xuan, Org. Electron. **13**, 2307 (2012).

[13]Y. Chen, J. Herrnsdorf, B. Guilhabert, A. L. Kanibolotsky, A. R. MacKintosh, Y. Wang, R. A. Pethrick, E. Gu, G. A. Turnbull, P. J. Skabara, I. D. W. Samuel, N. Laurand, and M. D. Dawson, Org. Electron. **12**, 62 (2011).

[14]E. B. Namdas, M. Tong, P. Ledochowitsch, S. R. Mednick, J. D. Yuen, D. Moses, and A. J. Heeger, Adv. Mater. **21**, 799 (2009).

[15]M. G. Ramirez, P. G. Boj, V. Navarro-Fuster, I. Vragovic, J. M. Villalvilla, I. Alonso, V. Trabadelo, S. Merino, and M. A. Díaz-García, Opt. Express **19**, 22443 (2011).

[16]A. E. Vasdekis, M. J. Wilkins, J. W. Grate, R. T. Kelly, A. E. Konopka, S. S. Xantheas, and T.-M. Chang, Lab Chip **14**, 2072 (2014).

[17]J. R. Lawrence, G. A. Turnbull, and I. D. W. Samuel, Appl. Phys. Lett. **82**, 4023 (2003).

[18]G. Heliotis, D. D. C. Bradley, G. A. Turnbull, and I. D. W. Samuel, Appl. Phys. Lett. **81**, 415 (2002).

[19]N. C. Greenham, I. D. W. Samuel, G. R. Hayes, R. T. Phillips, Y. A. R. R. Kessener, S. C. Moratti, A. B. Holmes, and R. H. Friend, Chem. Phys. Lett. **241**, 89 (1995).

[20]A. K. Bansal, A. Ruseckas, P. E. Shaw, and I. D. W. Samuel, J. Phys. Chem. C **114**, 17864 (2010).

[21]T. Wood, J. Le Rouzo, F. Flory, P. Coudray, V. R. Mastelaro, P. Pelissari, and S. Zilio, Opt. Eng. **52**, 094104 (2013).

[22]G. F. Barlow, K. A. Shore, G. A. Turnbull, and I. D. W. Samuel, J. Opt. Soc. Am. B **21**, 2142 (2004).